Chinese Journal of Aeronautics, (2015), 28(3): 649–658

Chinese Society of Aeronautics and Astronautics
& Beihang University

Chinese Journal of Aeronautics

cja@buaa.edu.cn
www.sciencedirect.com

Alleviation of spike stall in axial compressors utilizing grooved casing treatment

Reza Taghavi-Zenouz [a,*], **Sarallah Abbasi** [b]

[a] *School of Mechanical Engineering, Iran University of Science and Technology, Tehran 16846-13114, Iran*
[b] *School of Mechanical Engineering, Arak University of Technology, Arak 38181-41167, Iran*

Received 20 May 2014; revised 4 July 2014; accepted 5 March 2015
Available online 16 April 2015

KEYWORDS

Axial compressor;
Casing treatment;
Frequency spectrum;
Spike stall inception;
Tip leakage flow

Abstract This article deals with application of grooved type casing treatment for suppression of spike stall in an isolated axial compressor rotor blade row. The continuous grooved casing treatment covering the whole compressor circumference is of 1.8 mm in depth and located between 90% and 108% chord of the blade tip as measured from leading edge. The method of investigation is based on time-accurate three-dimensional full annulus numerical simulations for cases with and without casing treatment. Discretization of the Navier–Stokes equations has been carried out based on an upwind second-order scheme and k-ω-SST (Shear Stress Transport) turbulence modeling has been used for estimation of eddy viscosity. Time-dependent flow structure results for the smooth casing reveal that there are two criteria for spike stall inception known as leading edge spillage and trailing edge backflow, which occur at specific mass flow rates in near-stall conditions. In this case, two dominant stall cells of different sizes could be observed. The larger one is caused by the spike stall covering roughly two blade passages in the circumferential direction and about 25% span in the radial direction. Spike stall disturbances are accompanied by lower frequencies and higher amplitudes of the pressure signals. Casing treatment causes flow blockages to reduce due to alleviation of backflow regions, which in turn reduces the total pressure loss and increases the axial velocity in the blade tip gap region, as well as tip leakage flow fluctuation at higher frequencies and lower amplitudes. Eventually, it can be concluded that the casing treatment of the stepped tip gap type could increase the stall margin of the compressor. This fact is basically due to retarding the movement of the interface region between incoming and tip leakage flows towards the rotor leading edge plane and suppressing the reversed flow around the blade trailing edge.

* Corresponding author. Tel.: +98 77240540.
E-mail addresses: taghavi@iust.ac.ir (R. Taghavi-Zenouz), s_abbasi@iust.ac.ir (S. Abbasi).
Peer review under responsibility of Editorial Committee of CJA.

Production and hosting by Elsevier

1. Introduction

Compact engines are accompanied by compressors of lower numbers of stages and blades, which in turn causes aerodynamic loading of each stage to be increased, whilst keeping a compressor within a safe margin performance and a high efficiency.

http://dx.doi.org/10.1016/j.cja.2015.04.006
1000-9361

Rotating stall is known as one of the critical unsteady flow phenomena in dynamic compressors. This phenomenon, as a result of separation of flow from the blade surfaces, moves along the blade row in the circumferential direction. These separated circulatory flows, known as the stall cells, can produce blockages to the main flow within the blade passages. The rotating stall also changes pressure distributions on the blade surfaces in a periodic manner. Therefore, it would be responsible for noise generation and excitation of blade vibrations in different modes. The consequent unsteady forces may cause the compressor blades to be subjected to fatigue and fracture phenomena.

Control of flow instabilities is an effective method in improving a compressor's performance, which can be achieved by active or passive techniques. Of effective methods in active control of the blade tip unsteadiness can be referred to tip injection[1] and end wall bleeding or suction.[2] It is recognized that upstream injection[1] and downstream bleeding[2] can be led to increasing the stall margin of the compressor to a certain extent. Of the passive control methods for alleviation of the unsteadiness can be referred to casing treatment. Since the late 50 decades, this method has been known as an efficient method in enhancing the flow stabilities of compressors by improving the flow conditions near the blade tip and weakening the tip leakage vortex strength.[3–10]

Up to now, various types of casing treatments such as mounting slots or grooves over the rotor blade tip have been employed to enhance the compressor performance. Wilke and Kau[3] have described the impact of axial slots on the flow field in a transonic rotor blade row. They presented their results based on time-accurate three-dimensional numerical simulations of a high pressure compressor front stage with and without casing treatment. Two different axial positions of the casing treatment consisting of axial slots were tested for their impact on flow stability and efficiency. They clearly showed that the modified casing treatment stabilized the tip leakage vortex and reduced its influence on the flow inside the blade passage.

Another method of casing treatment, which is introduced as stepped tip gap, is similar to circumferential grooves and has been applied to both subsonic and transonic compressors.[4,5] Thompson et al.[5] have explored experimentally the effects of different stepped tip gaps and blade tip clearance levels on the performance of a transonic axial flow compressor, and found that for small and intermediate clearances, stepped tip gaps could improve overall pressure ratio, efficiency, and flow range for a wide range of operating conditions.

Rabe and Hah[6] studied experimentally and computationally the effectiveness of circumferential grooves on the stall margin of a transonic axial compressor. They claimed that the reason for the stall margin improvement was a reduction in flow incidence near the pressure side from the leading edge, which had dominant effects on flow structure. They also found that the shallow grooves were very effective in extending the stall margin.

Lu et al.[4] have reviewed the effects of stepped tip gaps on the flow field and performance of axial compressors based on experimental and computational methods, and performed parametric studies of blade tip clearance levels and step profiles of eight different geometries, considering flow simulations. Steady-state Navier–Stokes equations have been considered for their flow simulations. Shabbir and Adamczyk[10] have tried to numerically understand the physical mechanism responsible for improvement of the stall margin of a low speed rotor blade row due to existence of circumferential casing grooves and proved its effectiveness in enhancement of its operating range.

The flow field in the tip region of a rotor blade row is inherently unsteady and oscillatory. Hence, in addition to performing various kinds of casing treatments in enhancing the compressor stall margin, some researchers like Rae and Breuer,[11] Mailach et al.[12] and Zhang et al.[13] focused on studying the characteristics of this complex flow in details. Some investigations have been carried out to study the relation between the unsteady tip leakage flow and the spike stall inception as precursor of the fully developed rotating stall. The link between the tip leakage flow and the rotating stall has also been studied through three-dimensional simulations by some researchers.[14–16] Hoying et al. have considered movement of the tip leakage vortex towards the blade leading edge as a practical feature of the spike stall.[14] Vo et al. have introduced two transient phenomena in the tip leakage flow fields, known as leading edge spillage and trailing edge backflow at the blade tip, which are responsible for spike stall.[15]

Most of the researches are restricted to the casing treatment effects on the general performance of axial compressors. Unsteady flow field in the rotor blades tip region, particularly under high loadings, is not well studied up to now. In the current research work, the effects of grooved type casing treatment for the suppression of the spike stall is studied for an isolated axial compressor rotor blade row at near-stall conditions, utilizing unsteady numerical simulation of the tip leakage flow.

2. Model specifications and numerical scheme

The present investigation is carried out for a low speed isolated axial compressor rotor blade row subjected to other investigations experimentally or numerically.[17,18] Fig. 1 shows the model geometry and the computational grid structure. The model is comprised of 12 blades designed based on NACA-65 airfoil series. Geometric specifications of this rotor blade row are listed in Table 1.[17] The test Reynolds number based on the blade midspan chord length, the rotational speed of the rotor blade row, and the blade tip clearance size are 3.77×10^5, 1300 r/min, and 2 mm, respectively.

A grooved type casing treatment all around the compressor circumference has been considered. It is 1.8 mm in depth located between 90% and 108% of the blade tip chord measured from its leading edge (see Fig. 1(a)). In Fig. 1(a), C_x is the rotor blade tip axial chord length. This type of casing treatment has already been studied by Lu et al., but for a rotor blade row of a different geometry and aerodynamic performance.[4] They applied a grooved casing treatment for their rotor with different depths and widths for small, medium, and large tip clearance sizes. They concluded, from their experimental and numerical investigations, that the groove located within 90%–108% of the blade tip chord enhanced the performance of the blade for the medium tip gap size (1.9% of the blade tip chord length).

The well-known commercial flow solver package of Fluent has been used for the current study. The adopted solver is a three-dimensional, viscous, time-accurate code that utilizes a finite volume scheme for solution of the governing equations

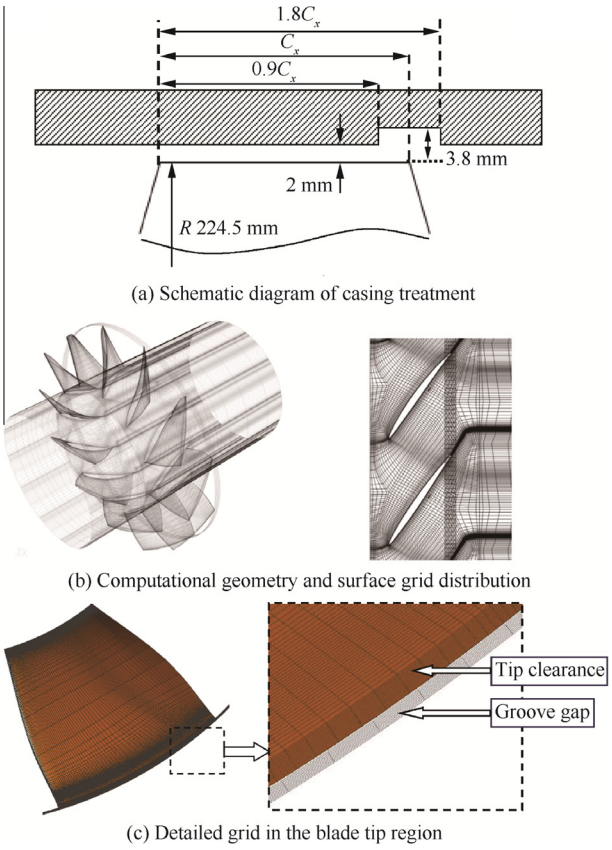

(a) Schematic diagram of casing treatment

(b) Computational geometry and surface grid distribution

(c) Detailed grid in the blade tip region

Fig. 1 Model geometry and computational grid structure.

Table 1 Model specifications.

Parameter	Value
Hub diameter (mm)	270
Hub to tip ratio	0.6
Tip clearance/blade chord (%)	1.7
Tip chord length (mm)	117.5
Midspan chord length (mm)	117.8
Blade tip solidity	1
Tip stagger angle (°)	56.2
Midspan stagger angle (°)	47.2

of continuity and momentum. In the present simulation, the upwind second-order discretization scheme has been used in order to reduce the effect of numerical diffusion on the solution. To solve the unsteady equations, the second-order implicit scheme has been applied for discretization of the governing equations. The k-ω-SST (Shear Stress Transport) turbulence model has been used to estimate the eddy viscosity.

As is shown in Fig. 1(b), the whole annulus passage has been modeled for a precise flow simulation. A multi-block structured grid system has been employed. The surface mesh structure is shown in the above figure. Each flow passage includes 74 streamwise, 50 spanwise, and 60 pitchwise nodes.

The mesh structure should have sufficient density especially in the blade tip clearance region and near the solid walls in order to resolve the flow characteristics precisely. The numbers of grids embedded in the tip clearance region of each compressor rotor blade is considered as 16, 68 and 15 in the spanwise, streamwise and pitchwise directions, respectively. The grooved region along the full annulus of the compressor passage consists of 10, 10 and 300 grids, distributed in the spanwise, streamwise and pitchwise directions, respectively. The mesh structure within the cavity is shown in Fig. 1(c).

The mesh density near the solid walls ensured y^+ values to be kept at less than 1, which enabled the viscous sub-layer to be resolved, precisely. Distribution of y^+ values on the blades and hub solid walls is introduced in Fig. 2. The whole grid system consisted of 35160000 cells.

Mesh independency studies have been performed for confidence of the right results. In this respect, different numbers of nodes have been distributed in the spanwise, pitchwise, and streamwise directions. The overall compressor performance was evaluated for different mesh structures consisted of a total number of cells ranged between 1440000 and 5832000. The relative difference between the loading factor values, calculated for these two extremes, was 2.56%. No considerable variations in the results have been observed for grid numbers exceeding 3516000. In this case, the mesh density near the solid walls ensured the y^+ values to be kept at less than 1, which enabled the viscous sub-layer to be resolved, precisely. The distribution of y^+ on the blades and the hub solid walls is shown in Fig. 2.

Therefore, a decision was made to consider the current numbers of grid cells for such an unsteady simulation to take advantage of shorter simulation time and limited computational resources.

When a time-accurate solution for stationary and moving part interaction is desired, the sliding mesh model should be used to compute the unsteady flow field. The sliding mesh model is the most accurate method for simulating flows in multiple moving reference frames. Each cell zone is bounded by at least one interface zone where it meets the opposing cell zone. The two cell zones will move relative to each other along the mesh interface.

The experimental data of Inoue et al.,[17] in terms of variations of the loading factor versus the flow coefficient, have been used to specify the numerical values of the flow variables on the boundaries of the computational domain. The inlet flow velocities for various conditions were extracted from the flow coefficient values, so the mass flow corresponding to each flow coefficient would be fixed since the flow is incompressible.

Since the overall pressure ratio of the test compressor is too low (due to its low rotational speed) and the outlet boundary position is considered so downstream, the outlet static pressure values would be very close to the atmospheric pressure. To find the outlet pressure distribution, the well-known radial equilibrium law was used on the outlet boundary with a starting point of the atmospheric pressure located on the compressor hub.

No-slip and adiabatic wall conditions were imposed all over the solid walls. Adapted time step has been considered too short for capturing flow phenomena precisely.

In the unsteady simulation process, the time step was chosen in such a way that one blade passing to be completed in 120 steps. This, in turn, corresponded to 1440 time steps for completion of one full rotor revolution. Since the angular velocity of the rotor was 1300 r/min, one revolution was completed in 4.6×10^{-2} s. As a result, a time step of 3.2×10^{-5} s was used in the present study. Accordingly, adopted sampling frequency is about 31 kHz while the blade passing frequency is 260 Hz. The CFL (Courant–Friedrichs–Lewy) number varied

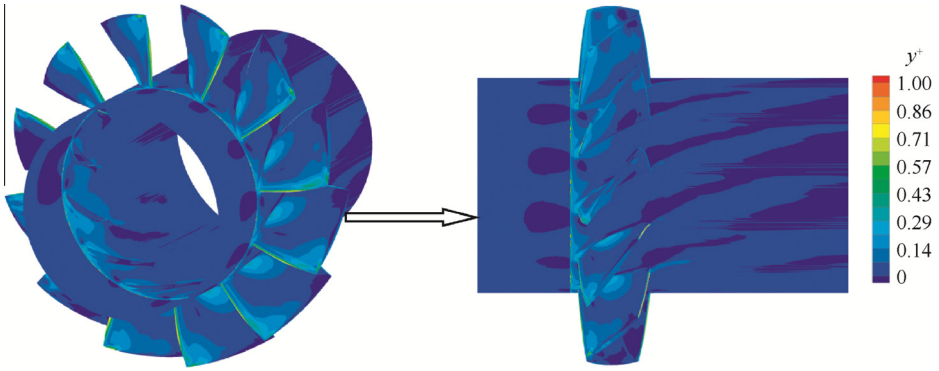

Fig. 2 Distribution of y^+ on the blades and the hub solid walls.

between 1 and 4. In the present work, 20 inner iterations were performed at each time step.

The residual values of the main governing equations approaching to around 10^{-7} were used as the convergence criterion in the numerical simulation process. As a complementary convergence criterion, statistical steady state monitoring of the flow variables at some selected points distributed on the blade surface (introduced in Section 4) was also carried out.

3. Results and discussion

3.1. Blade row performance

The blade row performance map, in terms of stage loading coefficient is shown in Fig. 3. In Fig. 3, ψ is total pressure rise coefficient, η is rotor blade row efficiency and φ is flow coefficient; Num-smooth and Num-CT refer to the numerical results of the smooth and treated casings, respectively. Good agreement between numerical and existing experimental results[17] can be observed. Casing treatment results are also superimposed in this figure.

It can be concluded that casing treatment has augmented the efficiency and the loading coefficient, indicating improvement in the blade row performance.

3.2. Tip leakage flow characteristics

Vo et al. showed that the leading edge spillage and the trailing edge backflow were two necessary criteria for inception of the spike stall.[15] These criteria are schematically demonstrated in Fig. 4.

In the resent research work, the method of investigation is based on time-accurate three-dimensional full annulus numerical simulations for cases of with and without casing treatment. Unsteady simulations are carried out for different mass flow rates at near-stall conditions. Based on the results obtained from the analyses, it has been recognized that, in the smooth casing, these two criteria for the stall inception occur at $\varphi = 0.36$.

All results, presented for both the smooth and treated casings, are extracted from unsteady numerical simulations. RMS values of unsteady fluctuations of the static pressure coefficient c_{prms} on 97% span stream-surface are presented in Fig. 5(a) and Fig. 5(b) for the smooth and treated casings, respectively. Results are presented for isometric and blade-to-blade views. Referring to these figures, the trajectory of vortices and their impingement regions to the adjacent blades can be recognized. The actual simulation point is stall inception point at $\varphi = 0.36$ on the performance map. Focusing on Fig. 5, it can be observed that, in contrast of the treated casing results, the RMS values are not identical for all the passages in the smooth

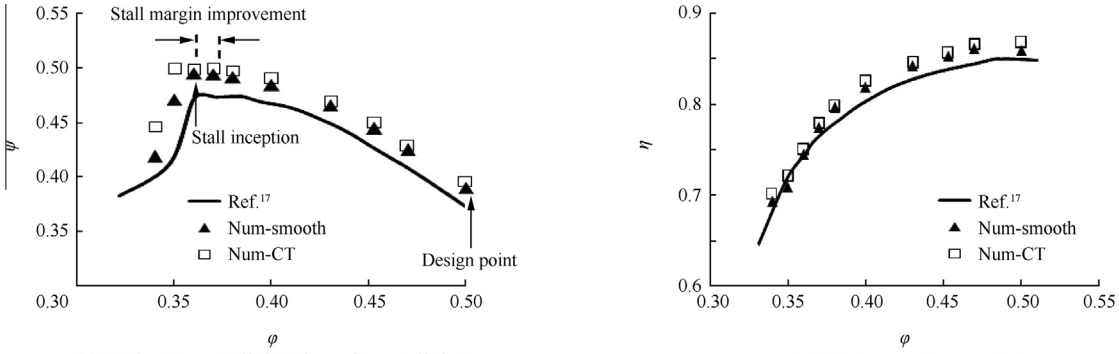

(a) Total pressure coefficient rise vs flow coefficient

(b) Efficiency vs flow coefficient

Fig. 3 Compressor blade row performance map.

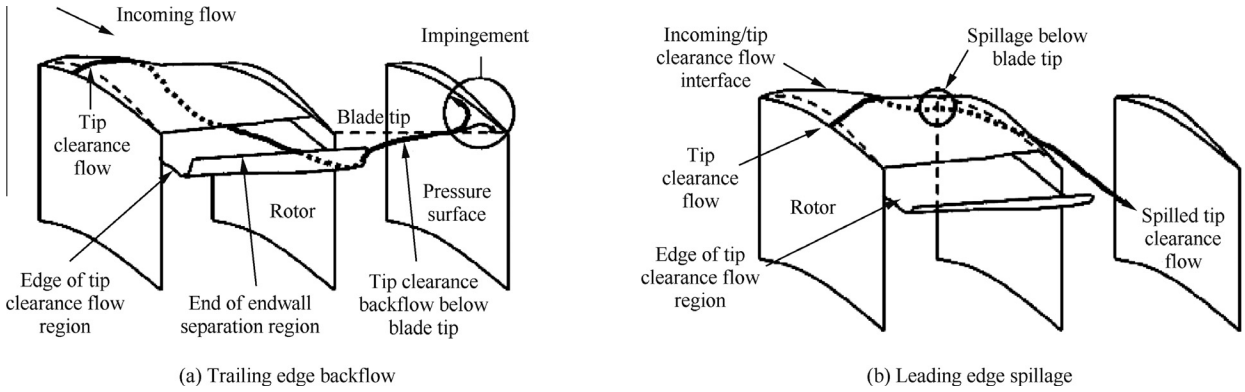

(a) Trailing edge backflow

(b) Leading edge spillage

Fig. 4 Schematic representation of two necessary criteria for spike stall inception.[15]

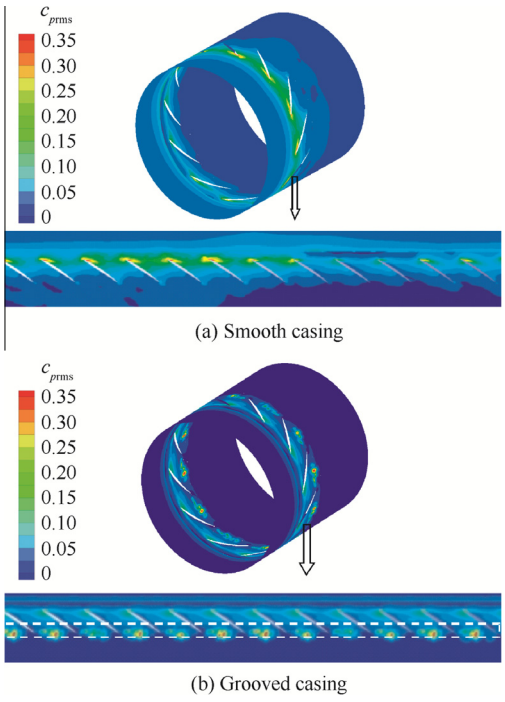

(a) Smooth casing

(b) Grooved casing

Fig. 5 Unsteady fluctuations of static pressures on 97% span stream-surface.

casing. These discrepancies are basically due to the difference in the strengths of the tip leakage vortices. Comparison between Fig. 5(a) and Fig. 5(b) reveals the fact that casing treatment has caused the strengths of tip leakage vortices to decrease. However, the unsteadiness at the stepped gap interface has strongly increased because of the interaction between axial and radial flows. This latter event is highlighted within a dashed rectangle in Fig. 5(b).

Results of the axial velocity coefficient c_{av} at 97% span stream-surface are shown in Fig. 6 for the smooth and grooved casings. For a better demonstration of the low-energy and reverse flow regions, the contours with just negative values are shown in the center of Fig. 6. The location of the reversed flow is marked by a circle in this figure. For better clarity, streamlines are shown in one of the reversed flow zones in this figure.

It can be clearly seen in these figures that the reversed flows have occurred in most passages for the smooth casing. It is necessary to emphasize that in two passages, this status is strongly intensified which leads to a significant blockage to the main stream. This non-uniform flow deficit is called stall cell. Results of Fig. 6(b) and comparing them with those of Fig. 6(a) reveal the fact that the grooved casing has extremely decreased the reversed flow, which is of course a beneficial task. It is clear that the number of stall cells has increased for the treated casing, but with smaller sizes in comparison to the untreated case.

To find out the propagation characteristics of the stall cells in both radial and circumferential directions, the contours of the negative axial velocities at a 50% axial chord cross plane are shown in Fig. 7. Results are illustrated for three instants including inception of the spike stall and the subsequent 1 and 3 rotor revolutions after this. In Fig. 7, N refers to the number of rotor revolutions after the spike stall commencement. It can be observed that one stall cell occupies about 25% of the spanwise passage in the smooth casing. By further rotation of the rotor, at $N = 3$, two dominant stall cells have appeared. The stall cells rotate at a speed lower than that of the rotor blades in the relative frame system and in an opposite direction. On the other hand, in the grooved casing, the blocked region contains many small stall cells but forms a thin band near the casing (see Fig. 7(b)).

Based on the results presented in Fig. 7, it can be concluded that the casing treatment has prevented the propagation of the stall cells in the radial direction. In other words, the main effect of casing treatment would be distribution of small reversed flows in all passages instead of existence of concentrating large stall cells in one passage.

3.3. Stall margin improvement

Obviously, study of the fluid structure for the untreated casing can provide fundamental information which can be used for a better description of effectiveness of the casing treatment. Fig. 8 illustrates contours of the relative total pressure coefficient c_{rpt} for both cases. These results can be used to demonstrate the interface plane between the tip leakage flow and the main inflow. Since the tip leakage flow does not take any shaft work as the energy input, its relative total pressure values are lower than those of the main inflow. Therefore, the region influenced by the tip leakage flow can be easily identified in the

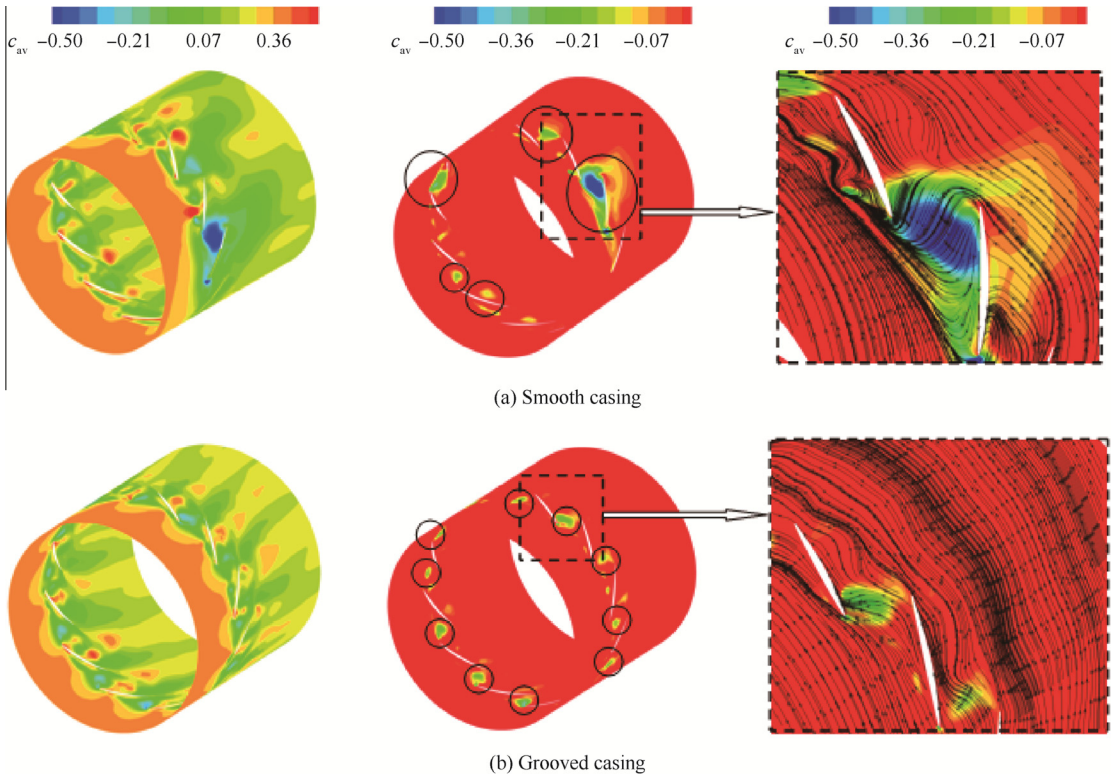

Fig. 6 Axial velocity coefficient at 97% span stream-surface.

relative total pressure contours. Ahead of the plane interface, it belongs to the incoming flow, but after that, it would be dominated by the tip leakage flow. The trajectory of the incoming/tip clearance flow interface results from a balance between the momentum of the incoming flow and that of the tip clearance flow. As the incoming mass flow reduces, the axial momentum of the incoming flow decreases, while the momentum of the tip leakage flow increases due to the increased blade loading. On the other hand, the momentum of the tip leakage flow increases due to the increment of the blade loading. Streamline patterns are also superimposed in these figures for a better recognition of the spike stall inception.

As can be observed in Fig. 8(a) for the smooth casing, the trajectory of the incoming/tip clearance flow interface is completely detached from the blades' leading edges, and a forward spillage of the tip clearance flow has occurred. In addition, streamlines show reversed flow at the trailing edge plane. Therefore, it can be concluded that the two necessary criteria in the flow field, responsible for the stall inception (i.e., leading edge spillage and trailing edge backflow), exist. In other words, the spike stall has occurred for the smooth casing under the proposed flow conditions.

Results presented in Fig. 8(b) for the treated casing demonstrate that the incoming/tip clearance flow interface has moved towards the rotor leading edge plane. This leads to formation of a weak leading edge spillage which has occurred only in a particular passage without creation of any trailing edge backflow.

Focusing on Figs. 6–8, one can deduce that the inclusion of casing treatment can cause the axial momentum of the incoming flow at the blade tip to increase significantly. Adding the streamlines in Fig. 8 helps in easy recognition of the incoming/tip clearance flow interface, so it is clear that the tip clearance flow trajectory sweeps towards the blades trailing edge plane in the grooved casing. It can be observed in Fig. 8(a) that two relatively large vortices are formed close to the blade leading edge within the flow passage, where the spike stall has occurred. In contrast, in the treated casing, the tip leakage vortex has been formed further downstream and its size has reduced (see Fig. 8(b)).

4. Frequency analysis

The unsteady nature of the tip leakage flow and stall cells can be studied through surveying the instantaneous surface pressure signals. Therefore, in order to accurately quantify the frequency of the unsteady tip leakage flow, a decision was made to utilize frequency analysis. It leads to getting a deeper insight into the flow characteristics during the stalling process and the role of the grooved casing in weakening the tip flow unsteadiness.

In this respect, a number of pseudo monitoring points were distributed on the casing and the blade pressure side at 97% span. These points were evenly spaced within 10%–90% of the blade chord length measured from its leading edge along the main stream direction. The points on the casing wall (designated by C_1 to C_7) are called fixed monitoring points, while those on the blades (designated as P_1 to P_7) are called rotating monitoring points. The measuring points of C_1 to C_7 and P_1 to P_7 are introduced in Fig. 9.

The sampling of the numerical pressure signals has been started after the final convergence of the numerical solution. The frequency spectrum results for the smooth and treated

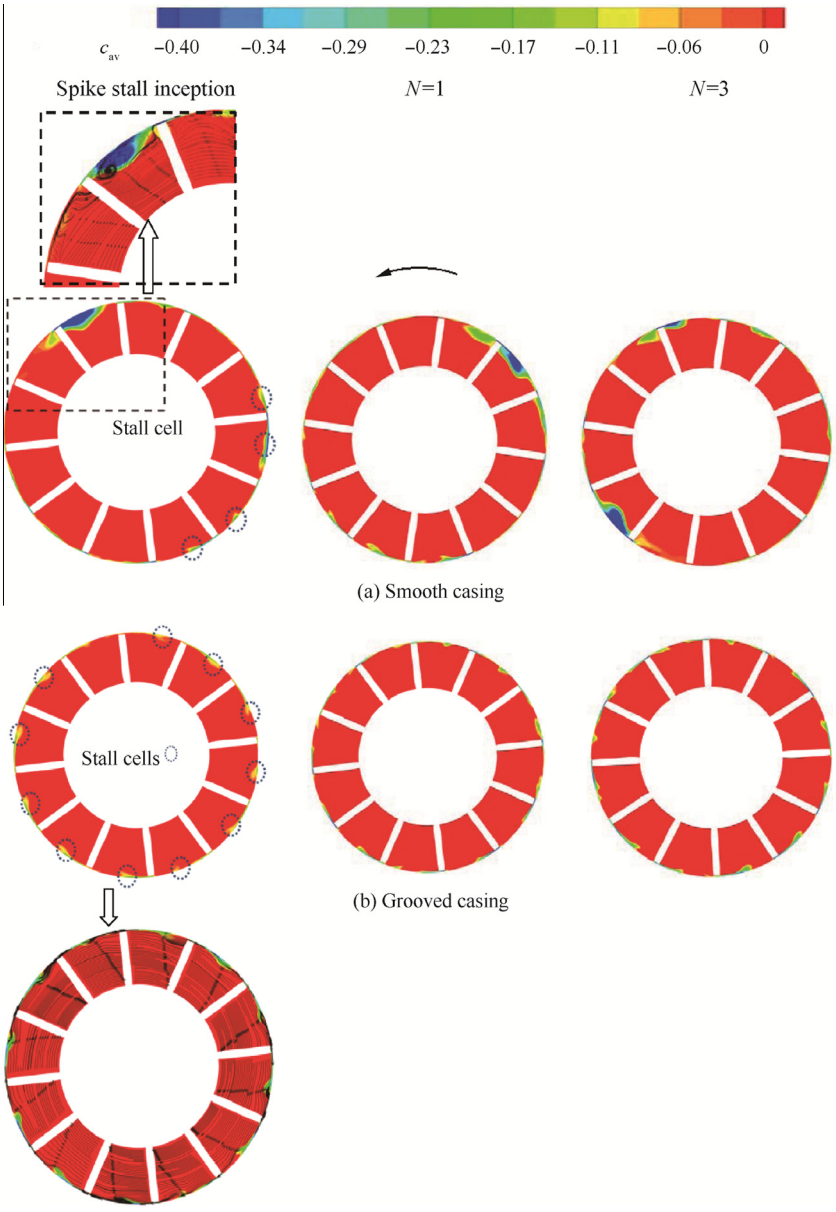

Fig. 7 Contours of axial velocity coefficient at 50% axial chord cross plane.

casings are shown in Figs. 10 and 11, respectively. These results are in terms of the PSD (Power Spectral Density) of the instantaneous pressure versus the flow frequency normalized with the blade passing frequency (BPF). It can be deduced from Fig. 10(a), presented for the smooth casing, that the dominant frequency for the fixed monitoring points is less than 0.2BPF. Obviously, the BPF does not appear in the FFT results while dealing with the rotating monitoring points (see Fig. 10(b)). In the latter case, the dominant frequency is about 0.1BPF. Several peaks of considerable magnitudes can be observed at each chordwise position, indicating the occurrence of the spike stall. This conclusion is in a good agreement with the results of Zhang et al.[13] and Vo et al.,[15] which have shown that the periodic characteristics of the tip leakage flow can be recognized by existence of some peaks in the frequency spectrum at the near-stall condition. Zhang et al.[13] have shown that the self-induced unsteadiness is caused by the interaction of the main inflow with the tip leakage flow and fluctuates with a frequency lower than the blade passing frequency. In addition, Vo et al.[15] have illustrated that the tip leakage vortex frequencies tend to move towards lower values with higher amplitudes during the stall inception conditions. They have also showed that at the stall inception condition, the maximum fluctuations of flow occur near the blade leading edge.

Fig. 11 presents the FFT results of the pressure signals for the treated casing. In this case, the dominant frequency for the fixed monitoring points (after the BPF) is about 0.5BPF and 1.1BPF (see Fig. 11(a)). For the rotating monitoring points, the dominate frequency can be observed as 0.4BPF (see Fig. 11(b)). Therefore, in similarity to the smooth casing, these results indicate the existence of the flow unsteadiness in the tip region. Interaction between the flow in the blade tip region and the main inflow leads to the formation of the tip leakage vortex. In Fig. 8, it is shown that the tip leakage vortex has also

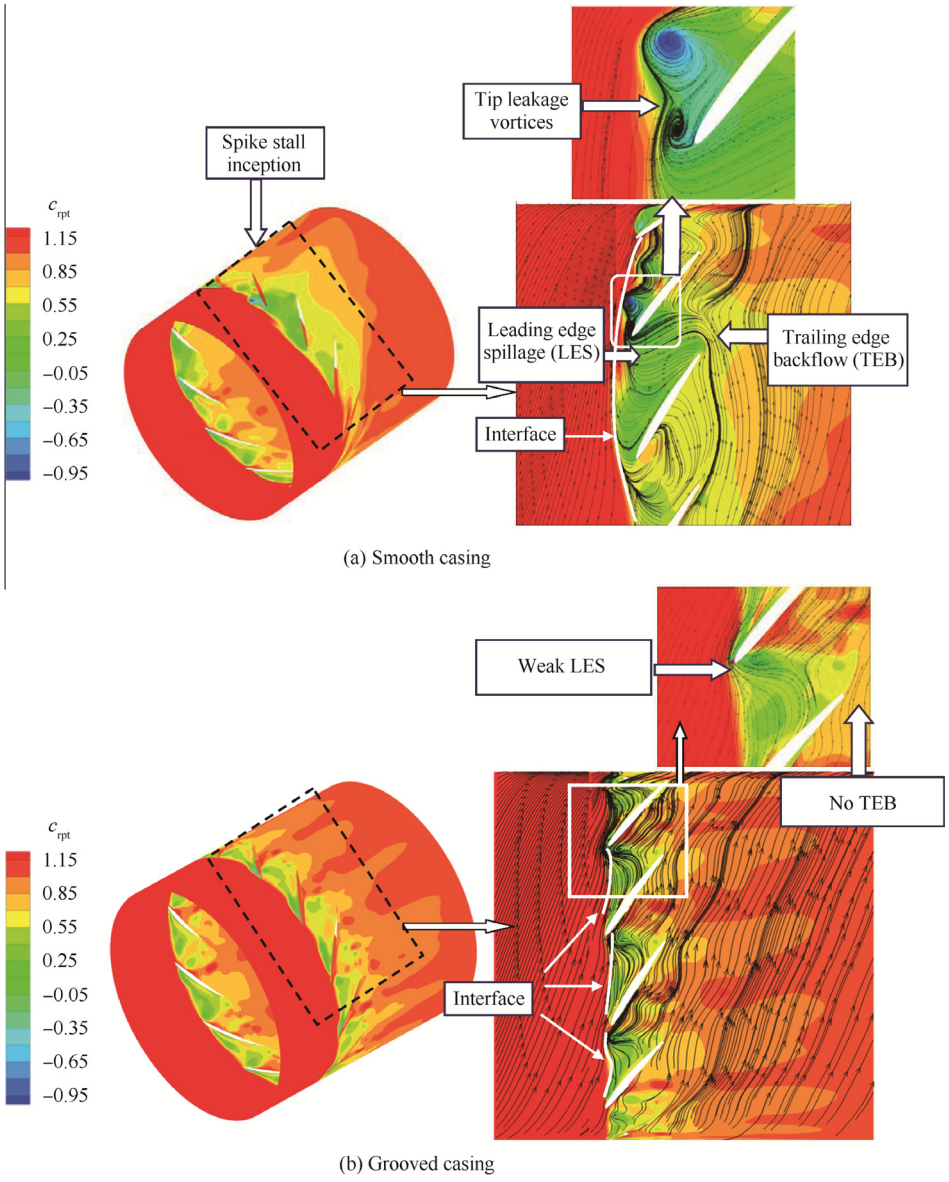

Fig. 8 Streamlines and relative total pressure contours at 97% span.

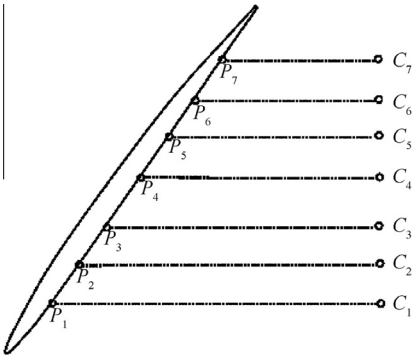

Fig. 9 Positions of the monitoring points in the rotor tip region.

occurred in the treated casing. The tip leakage vortex has moved from the blade leading edge towards the pressure side of the adjacent blade and has eventually dissipated. The process of formation of the tip leakage vortex until its dissipation happens within a specified time period. Referring to Fig. 5, one can detect that the unsteady pressure fluctuations originate from the blade leading edge and move towards the pressure side of the adjacent blade in both the smooth and treated casings. Therefore, it is recognized that the tip leakage vortex has also fluctuated in the treated casing, so the frequency of 0.4BPF appearing in Fig. 11(b) for the treated casing belongs to the tip leakage vortex flow.

In contrast to the smooth casing, no sign of the stall inception has been observed. Casing treatment has caused the dominant frequency of the tip leakage flow to increase and the amplitudes of the fluctuations to decrease. In other words, the flow field near the tip region of the blade is not strongly affected by the tip leakage flow for the treated casing. It can be concluded that this type of casing treatment has resulted in the improvement of the compressor stability in near-stall conditions.

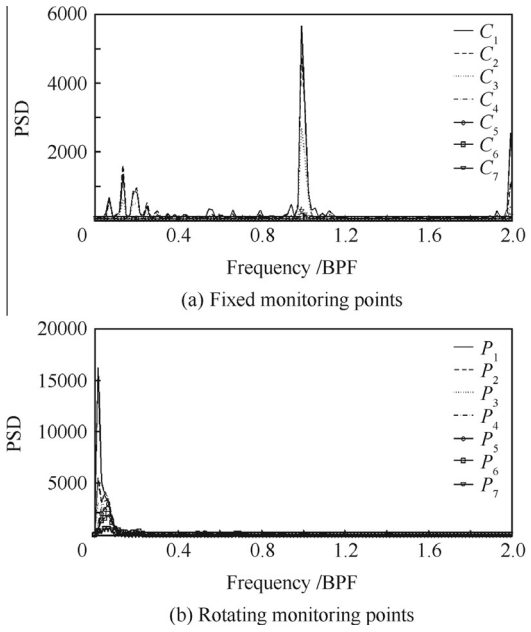

Fig. 10 Frequency spectrums in the rotor blade row tip region for the smooth casing.

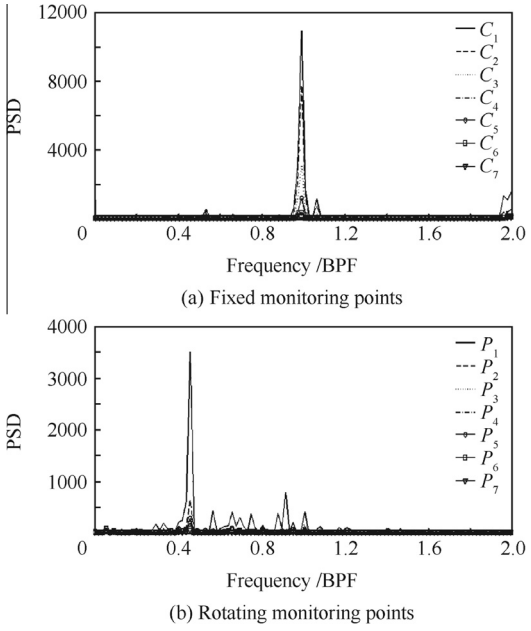

Fig. 11 Frequency spectrums in the rotor blade row tip region for the grooved casing.

As has already been mentioned in the frequency analysis section, it can be concluded that considering this type of casing through a design process can serve as an effective passive control mechanism for cases in near-stall conditions.

5. Conclusions

To understand the physical process associated with tip clearance and casing treatment, a numerical study has been done for an axial flow compressor rotor. A low-speed axial flow compressor with and without stepped tip gap casing treatment is investigated. The main conclusions drawn from this research work can be stated as follows.

(1) The unsteady simulation results for the smooth casing reveal that the two criteria for spike stall inception known as leading edge spillage and trailing edge backflow occur at specific mass flow rates in near-stall conditions.The smooth casing can be accompanied by large vortices, formed near the blade leading edge, indicating spike stall inception. Casing treatment of stepped tip gap type causes the axial velocity to increase and flow blockages and losses in total pressure to decrease. The treated casing of grooved type causes a tip vortex of a smaller size to be replaced further downstream. Grooved casing treatment can prevent the propagation of stall cells in the radial direction.

(2) It is found that the role of stepped tip gap casing treatment on stall suppression is linked to repositioning of the incoming/tip clearance flow interface towards blades' trailing edges and delaying the forward movement of the incoming/tip clearance flow interface to the leading edge plane. Therefore, in fact, for any compressor exhibiting short length-scale or spike type of stall inception, any strategy that delays one of the two proposed criteria for spike formation should be effective in extending the operating range. In present research, utilizing stepped tip gap is an effective method for spike stall alleviation.

(3) For the best aerodynamic performance of rotor blade row, casing treatment of the grooved type should be considered near the blades trailing edges. As a result, the spike stall suppresses by eliminating trailing edge backflow. In fact, the decline on the leading edge spillage should attribute to the improved flow capacity of the trailing edge.

(4) Frequency analyses of static pressure signals show that the dominant frequency in the grooved casing is about 0.5BPF and 1.1BPF for fixed monitoring points set on the casing. While in the smooth casing, this frequency is reduced to about 0.2BPF with higher amplitude. It means that the flow field near the tip region of a blade is not affected by the tip leakage flow for the treated casing due to suppression of the stall inception.

Acknowledgement

Financial support of the Aerodynamics and Compressible Turbomachinery Research Laboratory at Iran University of Science and Technology is highly appreciated.

References

1. Suder KL, Hathaway MD, Thorp SA, Strazisar AJ, Bright MB. Compressor stability enhancement using discrete tip injection. *J Turbomach* 2001;**123**(1):14–23.
2. Merchant A, Kerrebrock JL, Adamczyk JJ, Braunscheidel E. Experimental investigation of a high pressure ratio aspirated fan stage. *J Turbomach* 2005;**127**(1):43–51.
3. Wilke I, Kau HP. A numerical investigation of the influence of casing treatments on the tip leakage flow in a HPC front stage.

Proceedings of ASME Turbo Expo 2002: power for land, sea, and air; 2002 Jun 3–6; Amsterdam, the Netherlands. New York: ASME. p. 1155–65.
4. Lu X, Zhu J, Chu W. Numerical and experimental investigation of stepped tip gap effects on a subsonic axial-flow compressor rotor. *Proc IMechE Part A J Power Energy* 2005;**219**(8):605–15.
5. Thompson DW, King PI, Robe DC. Experimental investigation of stepped tip gap effects on the performance of a transonic axial-flow compressor rotor. *J Turbomach* 1998;**120**(3):477–86.
6. Rabe DC, Hah C. Application of casing circumferential grooves for improved stall margin in a transonic axial compressor. *Proceedings of ASME Turbo Expo 2002: power for land, sea, and air; 2002 Jun 3–6; Amsterdam, the Netherlands*. New York: ASME; 2002. p. 1141–53.
7. Hanley BK. Effect of circumferential groove casing treatment parameters on axial compressor flow range [dissertation]. Massachusetts: Massachusetts Institute of Technology; 2010.
8. Qiang XQ, Zhu MM, Teng JF. Effect of circumferential grooves casing treatment on tip leakage flow and loss in a transonic mixed-flow compressor. *J Theor Appl Mech* 2013;**51**(4):903–13.
9. Ross MH. Tip clearance flow interaction with circumferential groove casing treatment in a transonic axial compressor [dissertation]. Notre Dame, IN: University of Notre Dame; 2013.
10. Shabbir A, Adamczyk JJ. Flow mechanism for stall margin improvement due to circumferential casing grooves on axial compressors. *J Turbomach* 2004;**127**(4):708–17.
11. Bae J, Breuer KS. Periodic unsteadiness of compressor tip clearance vortex. *Proceedings of ASME Turbo Expo 2004: power for land, sea, and air; 2004 Jun 14–17; Vienna, Austria*. New York: ASME; 2004.
12. Mailach R, Sauer H, Vogeler K. The periodical interaction of the tip clearance flow in the blade rows of axial compressors. *Proceedings of ASME Turbo Expo 2001: power for land, sea, and air; 2001 Jun 4–7; New Orleans, Louisiana*. New York: ASME; 2001.
13. Zhang H, Deng X, Chen J, Huang W. Unsteady tip clearance flow in an isolated axial compressor rotor. *J Therm Sci* 2005;**114**(3):211–9.
14. Hoying DA, Tan CS, Vo HD, Greitzer EM. Role of blade passage flow structures in axial compressor rotating stall inception. *J Turbomach* 1999;**121**(4):735–42.
15. Vo HD, Tan CH, Greitzer EM. Criteria for spike initiated rotating stall. *J Turbomach* 2008;**130**(1):011023.
16. Hah C, Rabe DC, Wadia AR. Role of tip-leakage vortices and passage shock in stall inception in a swept transonic compressor rotor. *Proceedings of ASME Turbo Expo 2004: power for land, sea, and air; 2004 Jun 14–17; Vienna, Austria*. New York: ASME; 2004.
17. Inoue M, Kuroumaru M, Fukuhara M. Behavior of tip leakage flow behind an axial compressor rotor. *J Eng Gas Turbines Power* 1986;**108**(1):7–14.
18. Furukawa M, Inoue M, Saiki K, Yamada K. The role of tip leakage vortex breakdown in compressor rotor aerodynamics. *J Turbomach* 1999;**121**(3):469–80.

Reza Taghavi-Zenouz is an associate professor at Iran University of Science and Technology. His main research interests are turbomachinery design and analysis.

Sarallah Abbasi is an assistant professor at Arak University of Technology. His main research interests are turbomachinery design and analysis.